LEARNING TO INITIATE AND REASON IN EVENT-DRIVEN CASCADING PROCESSES

Yuval Atzmon*, **Eli Meirom***, **Shie Mannor, Gal Chechik**
NVIDIA Research
{yatzmon, emeirom, smannor, gchechik}@nvidia.com

ABSTRACT

Training agents to control a dynamic environment is a fundamental task in AI. In many environments, the dynamics can be summarized by a small set of events that capture the semantic behavior of the system. Typically, these events form chains or cascades. We often wish to change the system behavior using a single intervention that propagates through the cascade. For instance, one may trigger a biochemical cascade to switch the state of a cell.

We introduce a new learning setup called *Cascade*. An agent observes a system with known dynamics evolving from some initial state. The agent is given a structured semantic instruction and needs to make an intervention that triggers a cascade of events, such that the system reaches an alternative (counterfactual) behavior. We provide a test-bed for this problem, consisting of physical objects.

We devise an algorithm that learns to efficiently search in exponentially large semantic trees. We demonstrate that our approach learns to follow instructions to intervene in new complex scenes.

1 INTRODUCTION

Teaching agents to understand and control their dynamic environments is a fundamental problem in AI. It becomes extremely challenging when events trigger other events. We denote such processes as *cascading processes*. Cascading processes are prevalent in man-made systems. For example, in assembly lines, when one task is completed, e.g., construction of gears, it may trigger another task, e.g. building the transmission system. Cascading processes are also abundant in natural environments, e.g. chemical reactions. A major goal with cascading processes is to intervene and steer them towards a desired goal. For example, in biochemical cascades, one tries to control chemical cascades in a cell by providing chemical signals.

This paper addresses the problem of reasoning about a cascading process and controlling its qualitative behavior. We describe a new counterfactual reasoning setup called "*Cascade*", which is trained via supervised learning. At *inference* time, an agent observes a dynamical system, evolving through a cascading process that was triggered from some initial state. The goal of the agent is to steer the system toward a different, counterfactual, configuration. That target configuration is given as a set of qualitative constraints about the end results and the intermediate properties of the cascade. To satisfy the goal, the agent may intervene with the system at a *single, specific point in time* by changing the state of one specific element (the "pivot").

Steering a cascading process is hard. In many cascading processes, a slight change in one part of the system can make a qualitative effect on the outcome. This may lead to an exponential number of potential cascades. This "butterfly effect" (Lorenz, 1993) is typical in cascading systems.

Technical insights. Our approach is based on two key ideas. First, instead of modeling the continuous dynamics of the system, we reduce the search space by focusing on a small number of discrete, semantic events. In a billiard game, these events would be collisions of balls. To do this, we design a representation called an "*Event Tree*" (Figure 2). We build a tree of possible future events, where the root holds the initial world-state. Each child node corresponds to a possible future subsequent event from its parent. Our second idea is to learn how to efficiently search over the event tree. This is critical because the tree grows exponentially with its depth. We learn a function that assigns scores to tree nodes conditioned on the instruction and use these scores to prioritize the search. We also derived a Bayesian correction term to guide the search with the observed cascade.

*Equal contribution

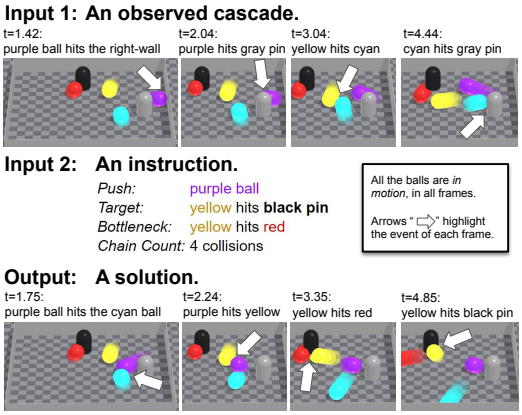

Figure 1: **An experimental test bed for the *Cascade* setup**. **Input 1** (the unsatisfied cascade): A set of balls is observed *moving* in a confined space, colliding with each other, with walls, and with static pins (grey & black). Collisions yield a cascade of events (arrows). **Input 2**: A complex instruction describes a desired "counterfactual" cascade of events and its constraints. **Output** (the satisfied cascade): The agent intervenes and sets the (continuous, 2D) initial velocity of the purple ball (the "pivot") to achieve the goal, *satisfying the constraints*. Only keyframes are shown. See full videos here: `https://youtu be/u1Io-ZWC1Sw` (Anonymous)

Modelling system dynamics with forward models. A forward model describes the evolution of the dynamic systems in small time steps. There is extensive literature on learning forward models from observations in physical systems (Fragkiadaki et al., 2016; Battaglia et al., 2016; Lerer et al., 2016; Watters et al., 2017; Janner et al., 2019). Recent work also studied learning forward models for cascades (Qi et al., 2021; Girdhar et al., 2021). However, once the forward model has been learned, the desired initial condition of the system is found by an exhaustive search. Here, we show that exhaustive search fails for complex cascades and with semantic constraints (Section 4). Therefore, our paper focuses on *learning to search*, rather than on *learning the forward model*.

Contributions. This paper proposes a novel approach for learning to *efficiently search* for a complex cascade in a dynamical system. Our contributions are: (1) A new learning setup, *Cascade*, where an agent observes a dynamical system and then changes its initial conditions to meet a given semantic goal. (2) Learning a principled probabilistic scoring function over a semenatic *Event Tree*, for searching efficiently over the space of interventions. (3) A Bayesian formulation leveraging the observed cascade to guide the search in the event tree toward a counterfactual outcome.

Related work: PHYRE, Virtual Tools, and CREATE Bakhtin et al. (2019); Allen et al. (2020); Jain et al. (2020) are benchmarks for physical reasoning. Their setup is a sequential decision reinforcement learning setup, allowing exploration and multiple retries, which are not allowed in our setup. Second, in the prior benchmarks, all tasks have to satisfy the same final goal. Finally, the current paper focuses on the *search* problem, rather than on learning a forward model. Roussel et al. (2019) focused on robustly tuning the simulator configuration given a known cascade. Our work focuses on *finding* a cascading configuration given a partial semantic description. Pertsch et al. (2020); Jayaraman et al. (2019) learned from video data to predict key-frames, but rely on a visual end frame.

2 THE "*Cascade*" LEARNING SETUP

Cascade is a supervised learning problem. At *inference*, the agent is provided with a dynamical system and two inputs: (1) A sequence of events called the "observed cascade" together with the respective initial condition of the system. (2) An instruction that describes desired semantic properties ("constraints") of the solution. The observed cascasde does not satisfy the instruction. The agent is asked to intervene by controlling the state of one "pivot element" at a specific point in time.

At the *training* phase, we are *only given* "successful" labeled samples. Each sample consists of (1) an instruction; and (2) the initial state of the system except the controllable pivot. The "label" (y) of each sample is the initial state of the pivot, which yields the desired behavior of the system. During training, we do not provide examples of failing sequences together with a successful sequence. *At test time*, a novel sample is drawn, describing an unseen dynamical system and instruction; and an observed cascade roll-out that fails to fulfill the instruction.

Our test bed: We introduce a new simulated test bed that abstracts away from specific applications. An agent observes a physical world with several moving and static objects going through a cascade of events (Figure 1 top), and it is given a *complex* instruction "*Push: purple ball . . .* ". It then manipulates the direction and speed of the purple ball (Figure 1 bottom) manifesting a new cascading process that satisfy the complex set of constraints given by the instruction.

3 METHODS

The Cascade setup presents three major challenges: First, our model needs to identify semantic events, but simulations of dynamical systems typically follow fixed and small timesteps, which are indifferent to events. Second, the set of constraints and dynamical systems is compositional and large. The agent needs to generalize to different systems and configurations that were not observed in training. Third, We aim to use failed cascade examples which are only available during inference (counterfactual setup).

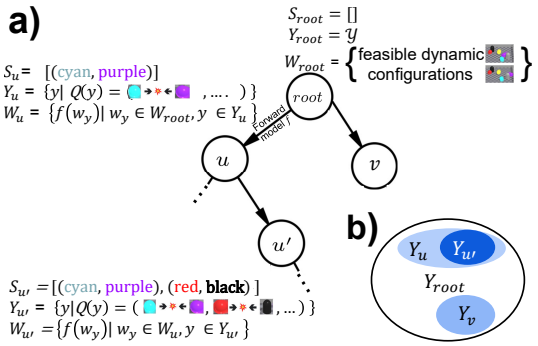

Figure 2: **(a)** The *Event Tree* data structure, illustrated according to our test-bed. S is the collision sequence of a node; Y is the intervention subset of a node; W is the node's world-state. See Section 3. **(b)** Tessellation of the intervention space.

To address the first challenge, we develop a representation that focuses on key "semantic" events of the dynamics (e.g., collisions). We build a tree of possible outcomes such that a path in the tree captures a realizable cascade of events. To address the second challenge, we learn a scoring function that assigns values to tree nodes conditioned on the instruction. At inference time, we use the predicted scores to search efficiently over the space of interventions. To address the third challenge, we develop a Bayesian formulation that allows to integrate the "counterfactual" information with the score predictions.

The *Event Tree*: A tree of possible futures The data structure we use to represent the search problem is the *Event Tree*. We represent the system behavior at the *semantic* level. These could be any key interactions between system components, e.g., a collision between two objects.

Each node corresponds to a *sequence* of semantic events, the node's *prefix* of semantic events. Each node has a unique prefix. The node's children correspond to realizable continuations of this sequence. Each node is also associated with a subset of interventions Y_u that share the same sequence of preceding events. Notably, while different interventions within a node result in the same prefix, they may result in different subsequent events after the prefix. The root node describes the set of possible interventions at $t = 0$, $\mathcal{Y}$, and its sequence of events S_{root} is empty. See Figure 2, top.

We propose *an event-driven forward model* $f(\cdot)$. It takes as input a state and outputs the next immediate semantic event. Expanding the tree can be viewed as a tessellation refinement of the intervention space $\mathcal{Y}$. At each step, we pick one cell and split it into multiple cells, where each child cell represents a different event that occurs after a shared sequence of events, represented by the parent cell. See Appendix I for details.

The score function. The number of nodes in such trees grows exponentially with the tree depth and exceeds billions of nodes even in our basic setup. We prioritize which node to expand by learning a *score* function for nodes, conditioned on the instruction g. There are three key challenges in learning a score function. First, we do not have ground-truth (target) scores for tree nodes. A naive choice for setting scores would set the score of the node that represents the ground-truth sequence to 1, and set all other scores to zero ("*All-or-None*"). However, this provides little guidance for searching the tree, as no signal is provided until the search hits the target node. Second, the training data contains only positive examples of correctly designed plans. Finally, we wish to leverage the information about the faulty observed cascade, but a faulty cascade is only observed during inference time.

To address these three challenges we design a principled probabilistic approach for the score function. We train our model to predict the likelihood that a sample from Y_u, when rolled out, will satisfy the instruction g, $V(u) = \Pr(Q(y) \text{ satisfies } g | y \in Y_u, g)$. Here, nodes on the path from the root to u^* are assigned *monotonically increasing* scores. The architecture is described in the appendix.

Counterfactual update for the score function. During inference, we observe a cascade that does not satisfy the instruction and are asked to retrospectively suggest a better solution. How can the observed cascade be used to find a solution? We use a Bayesian formulation and treat the model predictions as a *prior* for the true score, and the information about the observed cascade as *evidence*. Our model learns to estimate the *unconditioned* score function $V(\cdot)$. In the appendix, we show that we can express the Bayesian update of the scores in terms of $V(u^{obs}), V(u), V(u|S_{u^{obs}} \text{ doesn't satisfy } g) =$

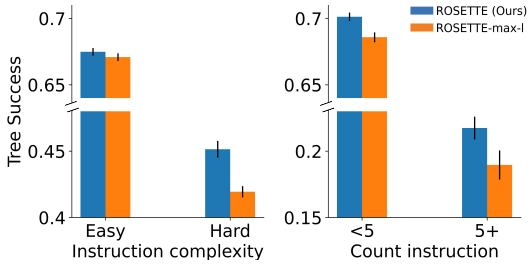

Figure 3: Comparing ROSETTE with ROSETTE-max-l for 2 levels of instruction complexity and for two levels of "count" instructions. ROSETTE performs better in complex scenarios.

	Tree Success	Simulator Success
Random	NA	$17.6 \pm 0.3\%$
Deepset Regression	NA	$18.4 \pm 0.5\%$
(Qi et al., 2021)	NA	$21.1 \pm 0.9\%$
Cross Entropy	NA	$20.9 \pm 0.4\%$
SEQUENTIAL	$52.4 \pm 0.6\%$	$43.1 \pm 0.3\%$
ROSETTE (Ours)	$\mathbf{60.8 \pm 0.3\%}$	$\mathbf{48.8 \pm 0.3\%}$

Table 1: **Success rates** of our approach and baselines. TREE is not applicable to the first three baselines since they do not use an event tree.

$V(u) - V(u^{obs}) \cdot fr(y^{obs}, y_u$, where $fr(u^{obs}, u) = \Pr(y \in Y_{u^{obs}} | y \in Y_u)$ is the probability that an intervention $y \in Y_u$ will result in sequence with prefix $S_{u^{obs}}$.

Inference Our agent searches the tree for the maximum scored node u_{MAX}. Then, it randomly selects an intervention from its intervention subset $y \in Y_{u_{MAX}}$. We limit the tree search to expand only 80 nodes, whereas in our test bed a full event tree, have billions of nodes. We consider two variants. **Maximum likelihood search:** The agent performs a tree search that expands the most likely nodes, and **Counterfactual search:** We apply the Bayesian correction term to the predicted score of every node along the observed sequence.

4 Experiments

We performed a detailed qualitative and quantitative analysis[1] (Appendix B). We compared our approach to SOTA baselines and human performance. An ablation study appears in the appendix.

Compared Methods: We compared the following methods. **(1) ROSETTE (Reasoning On SEmanTic TreEs)**: Our approach described in Section 3. Search uses the "counterfactual" variant of the tree search. **(2) ROSETTE-max-l.**: Like #1, but using "Maximum likelihood search". **(3) (Qi et al., 2021)**, The SOTA on PHYRE. For a fair comparison we replace their learned forward model by the full simulator of Makoviychuk et al. (2021). Hence, this baseline benefitted from using an exact forward model. **(4) Cross Entropy**: A standard planner (de Boer et al., 2005; Greenberg et al., 2022) that optimizes the objective function learned by compared method (3). Similarly to (3), this baseline had access to the exact model. **(5) Sequential**: Using a sequential representation for a tree chain, instead of a DAG. **(6) Deep Sets regression**: We embed the objects' initial positions and velocities using the permutation-invariant "Deep Sets" architecture (Zaheer et al., 2017), **(7) Random**: Sample interventions at random from an estimated distribution of ground-truth interventions.

Evaluation metrics: We use two success metrics, **Simulator success rate**: The success rate when rolling out the predicted intervention using a physical simulator (Makoviychuk et al., 2021). This metric mimics experimenting in the real world. **Tree success rate** (where applicable): Each node in the tree represents a sequence of events. A tree based algorithm selects a node. A "tree success" is when the selected node's sequence satisfy the instruction. This evaluates the performance of the score function and tree search, independently from errors introduced due to the forward model.

Table 1 describes the *Tree* and the *Simulator* success rates of ROSETTE and compared methods. ROSETTE achieves the highest success rate for both the "Tree" success rate (60.8%) and the "Simulated" success rate (48.8%). Achieving $\sim 80\%$ conversion rate from *Tree* to *Simulated*. The random baseline success rate is (17.6%), which is close to the performance of the regression model. We conjecture that the regression model fails, because it can't represent the outcomes as ROSETTE can. We further measured refinements of our metrics by conditioning on various properties of the instruction and scene (Fig. 3). We discuss the baselines' results in Appendix A.1.

Human evaluation. We conducted a user study with Amazon Mechanical Turk. We designed a game, where a player is given a video of the observed cascade and is asked to select one of 44 combinations of orientations (11) and speeds (4). ROSETTE achieves the highest average success rate ($43.3\% \pm 1.3\%$) compared to human success rate of $23.9\% \pm 2.6\%$. Appendix C, describes the experiment design and further analysis of the results.

[1]Examples: link #1, link #2, link #3.

REFERENCES

Kelsey R. Allen, Kevin A. Smith, and Joshua B. Tenenbaum. Rapid trial-and-error learning with simulation supports flexible tool use and physical reasoning. *Proceedings of the National Academy of Sciences*, 117:29302 – 29310, 2020.

Anton Bakhtin, Laurens van der Maaten, Justin Johnson, Laura Gustafson, and Ross B. Girshick. Phyre: A new benchmark for physical reasoning. In *Advances in Neural Information Processing Systems (NeurIPS)*, 2019.

Peter W. Battaglia, Razvan Pascanu, Matthew Lai, Danilo Rezende, and Koray Kavukcuoglu. Interaction networks for learning about objects, relations and physics. In *Advances in Neural Information Processing Systems (NeurIPS)*, 2016.

Peter W. Battaglia, Jessica B. Hamrick, Victor Bapst, Alvaro Sanchez-Gonzalez, Vinicius Zambaldi, Mateusz Malinowski, Andrea Tacchetti, David Raposo, Adam Santoro, Ryan Faulkner, Caglar Gulcehre, Francis Song, Andrew Ballard, Justin Gilmer, George Dahl, Ashish Vaswani, Kelsey Allen, Charles Nash, Victoria Langston, Chris Dyer, Nicolas Heess, Daan Wierstra, Pushmeet Kohli, Matt Botvinick, Oriol Vinyals, Yujia Li, and Razvan Pascanu. Relational inductive biases, deep learning, and graph networks, 2018.

P. T. de Boer, Dirk P. Kroese, Shie Mannor, and Reuven Y. Rubinstein. A tutorial on the cross-entropy method. *Annals of Operations Research*, 134:19–67, 2005.

Katerina Fragkiadaki, Pulkit Agrawal, Sergey Levine, and Jitendra Malik. Learning visual predictive models of physics for playing billiards, 2016.

Rohit Girdhar, Laura Gustafson, Aaron Adcock, and Laurens van der Maaten. Forward prediction for physical reasoning. *Time Series Workshop, ICML*, 2021.

Ido Greenberg, Yinlam Chow, Mohammad Ghavamzadeh, and Shie Mannor. Efficient risk-averse reinforcement learning. In *Advances in Neural Information Processing Systems*, 2022.

Aric Hagberg, Pieter Swart, and Daniel S Chult. Exploring network structure, dynamics, and function using networkx. Technical report, Los Alamos National Lab.(LANL), Los Alamos, NM (United States), 2008.

Ayush Jain, Andrew Szot, and Joseph J. Lim. Generalization to new actions in reinforcement learning. In *ICML*, 2020.

Michael Janner, Sergey Levine, William T. Freeman, Joshua B. Tenenbaum, Chelsea Finn, and Jiajun Wu. Reasoning about physical interactions with object-oriented prediction and planning. In *Proceedings of the International Conference on Learning Representations (ICLR)*, 2019.

Dinesh Jayaraman, Frederik Ebert, Alexei Efros, and Sergey Levine. Time-agnostic prediction: Predicting predictable video frames. In *International Conference on Learning Representations*, 2019. URL `https://openreview.net/forum?id=SyzVb3CcFX`.

D.P. Kingma and J. Ba. Adam: A method for stochastic optimization. In *ICLR*, 2015.

Adam Lerer, Sam Gross, and Rob Fergus. Learning physical intuition of block towers by example, 2016.

Edward N. Lorenz. *The Essence of Chaos.* UCL Press, London, 1993.

Viktor Makoviychuk, Lukasz Wawrzyniak, Yunrong Guo, Michelle Lu, Kier Storey, Miles Macklin, David Hoeller, Nikita Rudin, Arthur Allshire, Ankur Handa, and Gavriel State. Isaac gym: High performance gpu-based physics simulation for robot learning, 2021.

Judea Pearl. *Causality: models, reasoning and inference*, volume 29. Springer, 2000.

Karl Pertsch, Oleh Rybkin, Jingyun Yang, Shenghao Zhou, Konstantinos G. Derpanis, Kostas Daniilidis, Joseph J. Lim, and Andrew Jaegle. Keyframing the future: Keyframe discovery for visual prediction and planning. In *Learning for Dynamics & Control Conference*, 2020.

Haozhi Qi, Xiaolong Wang, Deepak Pathak, Yi Ma, and Jitendra Malik. Learning long-term visual dynamics with region proposal interaction networks. In *ICLR*, 2021.

Robin Roussel, Marie-Paule Cani, Jean-Claude Léon, and Niloy J. Mitra. Designing chain reaction contraptions from causal graphs. *ACM Trans. Graph.*, 38(4), 2019. ISSN 0730-0301. doi: 10.1145/3306346.3322977. URL https://doi.org/10.1145/3306346.3322977.

Benjamin Schäfer, Dirk Witthaut, Marc Timme, and Vito Latora. Dynamically induced cascading failures in power grids. *Nature Communications*, 9, 2018.

Nicholas Watters, Andrea Tacchetti, Theophane Weber, Razvan Pascanu, Peter Battaglia, and Daniel Zoran. Visual interaction networks. In *Advances in Neural Information Processing Systems (NeurIPS)*, 2017.

Manzil Zaheer, Satwik Kottur, Siamak Ravanbakhsh, Barnabás Póczos, Ruslan Salakhutdinov, and Alex Smola. Deep sets. In *NIPS*, 2017.

Giulio Zuccaro, Daniela De Gregorio, and Mattia Federico Leone. Theoretical model for cascading effects analyses. *International Journal of Disaster Risk Reduction*, 2018.

A ADDITIONAL RESULTS

Here we describe additional results and provide further discussion.

A.1 BASELINE RESULTS DISCUSSION

(Qi et al., 2021) baseline: We believe that the (Qi et al., 2021) baseline fails for three main reasons: (1) The baseline does not use an event-based representation. (2) It employs a classifier that is trained to provide an all-or-none signal, rather than guiding the search. The ablation study (Table **??**, right) demonstrates the importance of guiding the search (compare "Ours" 59.7% vs "All-or-None" 33.5%) (3) The baseline architecture cannot reason over the temporal DAG structure of a cascade, as our GNN can. The importance of capturing the DAG structure is demonstrated when comparing "Our" (60.8%) to the SEQUENTIAL baseline (52.4%) (Table **??**, left)

Existing Planners: We wish to provide further insight into why it is challenging to apply existing planners to this setup. The main challenge is that the optimization objective is given in semantic terms about the end goal. To apply a Cross-Entropy-Method (CEM) planner, we derive a corresponding objective function by training a classifier that checks if the goal was achieved for a given scene and plan. Specifically, we used the existing SoTA PHYRE classifier Qi et al. (2021). A main drawback is that classifiers provide an "all or none" signal, hence fail in guiding the planner through optimization. Conversely, our approach provides a score (Eq. **??**) that monotonically increases through the tree, and it is constructed to assist the search.

B QUALITATIVE EXAMPLES

Here we provide links to qualitative examples that we uploaded to YouTube. They are best viewed in $\times 0.25$ slow motion. The YouTube account we use is anonymous.

For each episode, we show a side-to-side video of the observed cascade, the ROSETTE successful case, and ROSETTE-max-l failure case. The instruction is displayed on top of each video.

- *Push: cyan ball, Target: blue hits red, Bottleneck: cyan hits bottom wall, Chain Count: 6*
  In this example, ROSETTE semantically follows the first 10 collisions (in chonological order) as in the observed cascade. It then diverges from the observed cascade, making the blue hit the red. The cyan pivot comes into play already on the 1st collision, and the agent adjusts its velocity such that it shall yield the goal. The ROSETTE-max-l baseline, hits the target, however it fails with the count constraint. The bottleneck collision occurs, but not on the chain from the pivot to the target. See the complete video here: `https://youtu.be/RCKFBRrCRw0`
- *Push: cyan ball, Target: green hits red, Bottleneck: purple hits red, Chain Count: 4*
  In this example, ROSETTE semantically follows the first 5 collisions (in chonological order) as in the observed cascade. The cyan pivot comes into play on the 3rd collision. It then diverges from the observed cascade, and follows another chain of events, making the purple hit the red, and concluding with the target hit within 4 collisions in the chain that started at the cyan ball. This task is too hard for the ROSETTE-max-l baseline, as it completely fails to satisfy the instruction. See the complete video here: `https://youtu.be/4s9MmY2J__I`
- *Push: green ball, Target: green hits cyan, Bottleneck: green hits purple, Chain Count: 5*
  In this example, ROSETTE semantically follows the first 6 collisions (in chonological order) as in the observed cascade. It then diverges from the observed cascade, making the green hit the purple, fulfiling the bottleneck constraint. The cyan pivot comes into play only on the 6th collision, and the agent adjusts its velocity such that both the target and the count constraint will by satisfied. The ROSETTE-max-l baseline, hits the bottleneck, however it fails to hit the target. See the complete video here: `https://youtu.be/iMedd_7YndQ`
- *Push: yellow ball, Target: cyan hits red, Bottleneck: purple hits red, Chain Count: -*
  In this example, ROSETTE semantically follows the first 5 collisions (in chonological order) as in the observed cascade. The yellow pivot comes into play only on the 5th collision, and the agent adjusts its velocity to satisfy the bottleneck constraint and the target. The

ROSETTE-max-l baseline, completely fails in this task. See the complete video here: https://youtu.be/QLMTD6R2Z54

- *Push: red ball, Target: blue hits red, Bottleneck: red hits bottom wall, Chain Count: -*
  In this example, ROSETTE semantically follows the first 4 collisions (in chonological order) as in the observed cascade. The red pivot comes into play already on the 2nd collision, and the agent adjusts its velocity to satisfy the bottleneck constraint and the target. The ROSETTE-max-l baseline, satisfy the bottleneck but does not satisfy the target. See the complete video here: https://youtu.be/vT1ivd1ECJs
- *Push: yellow ball, Target: blue hits purple, Bottleneck: blue hits right wall, Chain Count: -*
  In this example, ROSETTE semantically follows only the first 2 collisions (in chonological order) as in the observed cascade. The red pivot comes into play on the 3rd collision, and the agent adjusts its velocity to satisfy the bottleneck constraint and the target. The ROSETTE-max-l baseline, completely fails in this task. See the complete video here: https://youtu.be/rgzWBfx-LqY

Importantly, these examples demonstrate the usefulness of the observed cascade for tree search. ROSETTE followed the observed cascade along the part of the path that was useful to satisfy the instruction. It diverged from the path when necessary, and found a solution when long cascades were essential, while ROSETTE-max-l struggled.

Finally, we note that this observation is also quantitatively supported: As we show in Figure **??** and Figure A.4. When conditioning the Tree Success rate on producing long cascades, with *Chain count* constraint values greater or equal to 5, ROSETTE performs at $34.8 \pm 0.8\%$, while ROSETTE-max-l performs at $31.3 \pm 1.1\%$, showing $\sim 11.1\%$ improvement. For *Chain count* values smaller than 5, they are statistically equivalent $75.1 \pm 0.4\%$ and $75.4 \pm 0.4\%$.

C USER STUDY

We conducted a user study with Amazon Mechanical Turk (AMT) using 30 test episodes. We designed a game where a player (rater) is given a video of the observed cascade and is asked to select one of 44 combinations of orientations (11) and relative speeds (4) (magnitude of velocity). One combination of orientation and speed was aligned with the ground-truth solution, and the rest were spaced in relation to that solution. In an offline stage, we tested which of the *other* orientations and speeds satisfy the goal and included those as valid solutions. We allowed the players to freely replay the observed video. We paid 1$ per game.

Figure A.1 shows one test episode. The upper panel provides an instruction that states the goal of that specific episode. On the left, we provide a set of simple guidelines. The center panel provides the observed (failed) video. The right panel shows the initial frame, overlaid with the set of possible orientations and a set of HTML radio buttons to select the orientation and speed. The upper tab provides a set of four examples with solutions and explanations. Those examples are given in Figure A.2.

To maintain the quality of the queries, we only picked users with AMT "masters" qualification, demonstrating a high degree of approval rate over a wide range of tasks. Furthermore, we also executed a qualification test with a few curated episodes that are very simple. To qualify users, we made sure they do not randomly pick an answer by only qualifying users who completed 5 episodes and had a single error at most. Additionally, we deleted queries from one qualified user, who submitted answers at a rate of 3-4 episodes per minute, as we qualitatively observed that it should take 1-3 minutes to complete an episode.

Qualified users received a bonus of 0.5$, accompanied with the following message:

> Thank you for doing the qualification batch for our colliding balls game.
> Our full study is now online. You can start doing it. Please remember to PLAY THE VIDEO and use it to decide about your answer. And also, take another look at the examples, as they can provide more intuition about the task.

11 players have passed our qualification tests, playing 25 episodes on average. Table 2 compares the human success rate with ROSETTE and a Random baseline. Showing Average, Median and Best

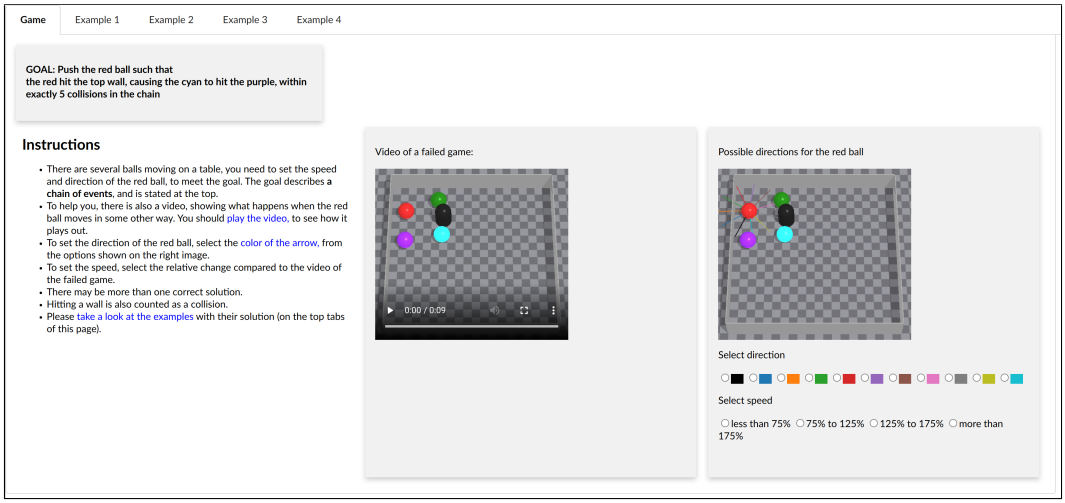

Figure A.1: One test episode of the user study. See Section C for details.

statistics. For the Median and Best statistics, we only included users who played a minimum number of 20 episodes (8 of 11 users).

	Average	Median	Best
Random	$17.6 \pm 1.1\%$		
Humans	$23.9 \pm 2.6\%$	25%	41.4%
ROSETTE	$\mathbf{43.3 \pm 1.3\%}$	**43.3%**	**46.7%**

Table 2: Success rate statistics for the user study. $\pm$ error denotes the standard error of the mean (S.E.M) across the samples.

D Additional Experimental Details

D.1 Hyperparameter Tuning

We train the model and baselines for 15 epochs. Batch size was set to 8192 to maximize the GPU memory usage. We use the PyTorch' default learning rate for Adam (Kingma & Ba, 2015) (0.001). For inference, we set $N_{observed}$ to 9, the maximal tree depth to 30, we sample 10^6 initial states and expand 80 nodes per episode which takes ~13 seconds. The GNN uses 5 layers, with a hidden state dimension of 128. Hyper parameters were tuned one at a time, during an early experiment on a validation set.

D.2 Random Baseline

We sample an intervention at random from an estimated distribution of ground-truth interventions. The distribution is estimated by calculating a 2D-histogram with 30×30, and approximating the distribution within each bin to be uniform.

D.3 Deepset regression Baseline

Overview: For the Deepset regression baseline, we embed the instruction and the initial world state to predict a continuous intervention. We use the permutation-invariant "Deep Sets" architecture (Zaheer et al., 2017), and use an L_2 loss with respect to ground-truth interventions in the "counterfactual" training samples.

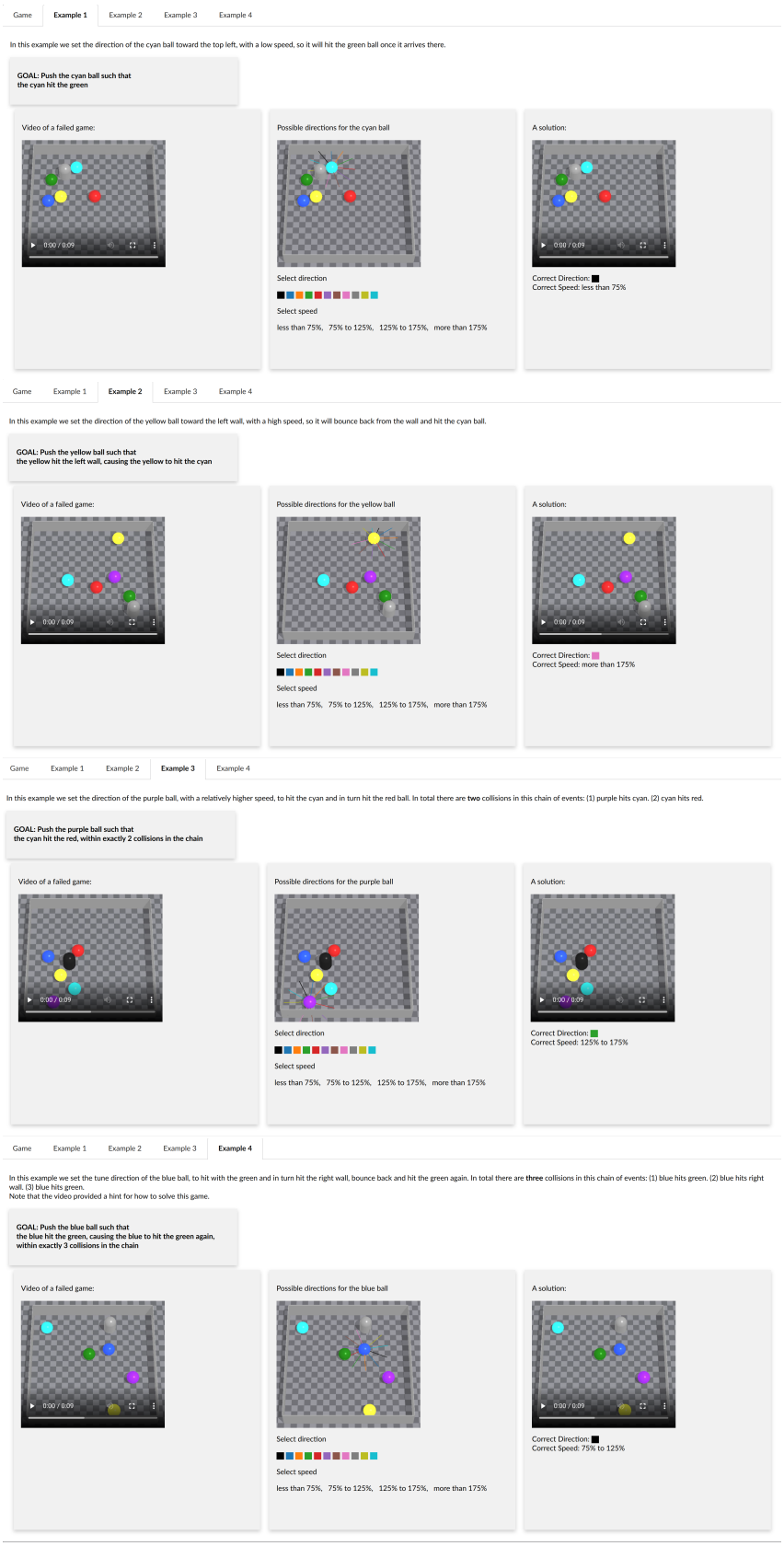

Figure A.2: Examples provided in the user study. See Section C for details.

The input to the Deepset architecture (Zaheer et al., 2017) is a set of feature vectors. Each feature vector corresponds to a dynamic or static object in the scene. The output is a vector $\in \mathbb{R}^2$, for predicting the controlled velocity of the pivot object.

Feature representation: Each feature vector in the set is represented by a concatenation of the following fields $[obj\_feat(o), instruction\_emb, position, velocity]$, where $obj\_feat(o)$ is defined by Eq. (1), $instruction\_emb$, is defined by Eq. (4), $position$, $velocity$ are the initial position and velocity of the object, as given by the observed cascade.

Labels and loss: For ground-truth labels, we use the ground-truth velocity of the solution. We use a L_2 loss comparing the ground-truth labels with the output of the Deepset architecture.

D.4 (QI ET AL., 2021) BASELINE

Overview: **Qi2021** is the state-of-the-art approach for solving PHYRE. It uses a learned forward model, a learned goal-satisfaction classifier, and exhaustive search. For a fair comparison with our analytic event-driven forward model, we replace their learned forward model by a full simulator (Makoviychuk et al., 2021).

Therefore, for the goal-satisfaction classifier, in each frame, we replace the set of input feature vectors coming from the region-proposal-interaction-network (RPIN) of (Qi et al., 2021) by a set of feature vectors corresponding to each object in the scene, and its kinematic state as given by the simulator. To condition the classifier on the goal, we concatenate the instruction representation to each feature vector.

Feature representation: Each feature vector of an object in a frame, is represented by a concatenation of the following fields $[obj\_feat(o), instruction\_emb, position, velocity, time]$, where $obj\_feat(o)$ is defined by Eq. (1), $instruction\_emb$, is defined by Eq. (4), $position$, $velocity$, $time$ are the respective readings from the simulator in the frame.

Positive and Negative examples: For training the goal-satisfaction classifier with positive examples, we use the simulation of the solution cascade. For negative examples, we use the simulation of the observed cascade.

Classifier Architecture: We use the classifier architecture of (Qi et al., 2021), as provided in their public implementation, with the following adaptations: (1) We replace the RPIN representation by the simulator-driven representation described above. (2) We allow replacing the last fully connected layer by a multi-layer-perceptron (MLP) (3) We allowed more than four equally spaced input frames.

Simulator configuration: The RPIN forward model is a fixed timestamp model, working at 1 frame-per-second. In the full simulator we used (Makoviychuk et al., 2021), we observed that it does not perform well in such a coarse-grained resolution, making objects to sometimes go through the walls. Therefore, we increased the simulator resolution to 10 frames-per-second.

Hyperparam search: We searched for the best hyper-parameters configuration that minimizes the validation loss over the following ranges: *Number of MLP hidden-layers* $\in [0, 1, \ldots 6]$, *Number of input frames* $\in [4, 6, 10, 20]$, *batch-size* $\in [128, 256]$. *Number of training epoch* was set according to early stopping on the validation set.

Finally, we used the following hyper-parameters to evaluate the model performance on the test set: *Number of MLP hidden-layers = 2*, *Number of input frames = 4* (as in (Qi et al., 2021) paper), *batch-size=128*, *Number of training epoch = 17*.

Evaluation: For evaluation, we randomly selected a subset of 208 episodes (10% of the test subset), because inference for a single episodes took $\sim$5.5 minutes.

D.5 CROSS ENTROPY BASELINE

Overview: The cross entropy method is a black box optimizer for solving optimization problems. We used (Qi et al., 2021) baseline's classifier as our objective function. At each step, we sampled 100 points and updated the sampling distribution based on their score. We have repeated this process for 100 iterations, and chosen the highest scored intervention for evaluation. Our code is based on a standard implementation Greenberg et al. (2022) of the cross entropy method.

For evaluation, we randomly selected a subset of 208 episodes (10% of the test subset), because inference for a single episodes took $\sim$4 minutes.

D.6 SEQUENTIAL BASELINE

We used the validation set to select the number of layers for this baseline, $\in [5, 10, 20, 30]$. There wasn't any significant difference when using 5 or 10 layers, and the success rate degraded for 20 or 30 layers. Therefore, we used 5 layers for evaluating performance on the test set.

D.7 ABLATION STUDY

We also carry a thorough ablation study. First, we explore alternative approaches to label node scores along the ground-truth sequence. *Linear*: Linearly increases the score by $V(u) = depth(u)/depth(u^*)$. *Step*: Give a fixed medium score to nodes along the sequence, and a maximal score to the target node: $V(u) = 0.5 + 0.5\mathbf{1}_{u^*}(u)$. *All-or-None*: Sets $V(u) = \mathbf{1}_{u^*}(u)$, this baseline is equivalent to the naive approach discussed in Section 3. Second, we compare the "Counterfactual" search to the "Maximum Likelihood" search by comparing their performance on **a dataset that includes more complex instructions.** This dataset includes a third constraint. We partition the dataset to "Easy" and "Hard" instructions, and compare these search methods on both types of instructions. We describe this dataset in the appendix. Last, we test how ablating parts of the instruction affects the ROSETTE model performance.

Ablation experiments: We highlight some key observations.**(1)** Table **??** shows the advantage of the probabilistic formulation of the score function (ROSETTE-max-l), compared to the several heuristics described in Section 4. The strongest baseline ("Linear") only reaches 48.7% vs. 59.7% for ROSETTE-max-l. **(2)** The *All-or-None* variant *establishes the value of event-drivenness*. It is similar to a classifier-based search like Qi et al. (2021), but uses an underlying event-driven forward model instead of a fixed time stamp model as in Qi et al. (2021). Comparing the two, we see that using EDFM with current SOTA improves the success rate, from 21% to 33.5%. (3) Comparing *ROSETTE-max-l* to the *All-or-None* variant further *establishes value of learning to search*, which improves the success rate from 33.5% to 59.7%. **(3)** Figure **??** quantifies the benefit gained by using "Counterfactual" search (ROSETTE) over Maximum-Likelihood search (Section **??**). ROSETTE shows a relative improvement of 7.7% (45.1% vs 41.9%) for complex instructions. **(4)** Table 3 (Appendix A) allows an in-depth examination of the strengths and weaknesses of ROSETTE, across 4 types of ablations, as described in Section 4. First, we observe that the sequential baseline can find target collisions that depend on a bottleneck collision, as well as ROSETTE. However, it fails with "count" instructions (46.3% vs 60.8%), since it has no capacity for that reasoning task. Second, we observe that ROSETTE is able to effectively use the instruction, as removing any part of the instruction hurts the success rate.

	UNCONSTRAINED	BOTTLENECK	COUNT	B & C
ROSETTE (OURS)	$76.5 \pm 0.8\%$	$68.5 \pm 1.0\%$	$60.8 \pm 0.7\%$	$49.5 \pm 0.5\%$
-COUNT	$75.8 \pm 0.9\%$	$68.4 \pm 0.8\%$	$6.1 \pm 0.6\%$	$17.1 \pm 0.5\%$
-BOTTLENECK	$76.4 \pm 0.9\%$	$21.5 \pm 1.1\%$	$61.1 \pm 1.2\%$	$34.1 \pm 0.7\%$
-COUNT -BOTTLENECK	$76.6 \pm 0.8\%$	$21.4 \pm 1.1\%$	$6.1 \pm 0.5\%$	$4.2 \pm 0.3\%$
-FULL	$60.8 \pm 0.5\%$	$32.7 \pm 0.9\%$	$11.7 \pm 0.5\%$	$6.6 \pm 0.1\%$
SEQUENTIAL	$77.9 \pm 0.4\%$	$66.9 \pm 1.3\%$	$46.3 \pm 1.3\%$	$36.5 \pm 1.3\%$

Table 3: **Ablation study**. In red, results that perform much worse than ROSETTE.

We further measured refinements of our metrics by conditioning on various properties of the instruction and scene (Fig. 3). **(1) Condition tree success rate on instruction type: Unconstrained:** The instruction only specifies target collisions. **Bottleneck:** also contains an "bottleneck" constraint. **Count:** contains a "count" constraint. **B&C:** contains both "bottleneck" and "count" constraints. **(2) Condition tree success rate on complex scenarios:** (2.1) Instructions with 2 or more constraints are marked as "Hard", and the rest as "Easy"; (2.2) Instructions with a "count" constraint value ≥ 5 are considered hard. Complex scenario conditioning was evaluated on the complex instruction dataset.

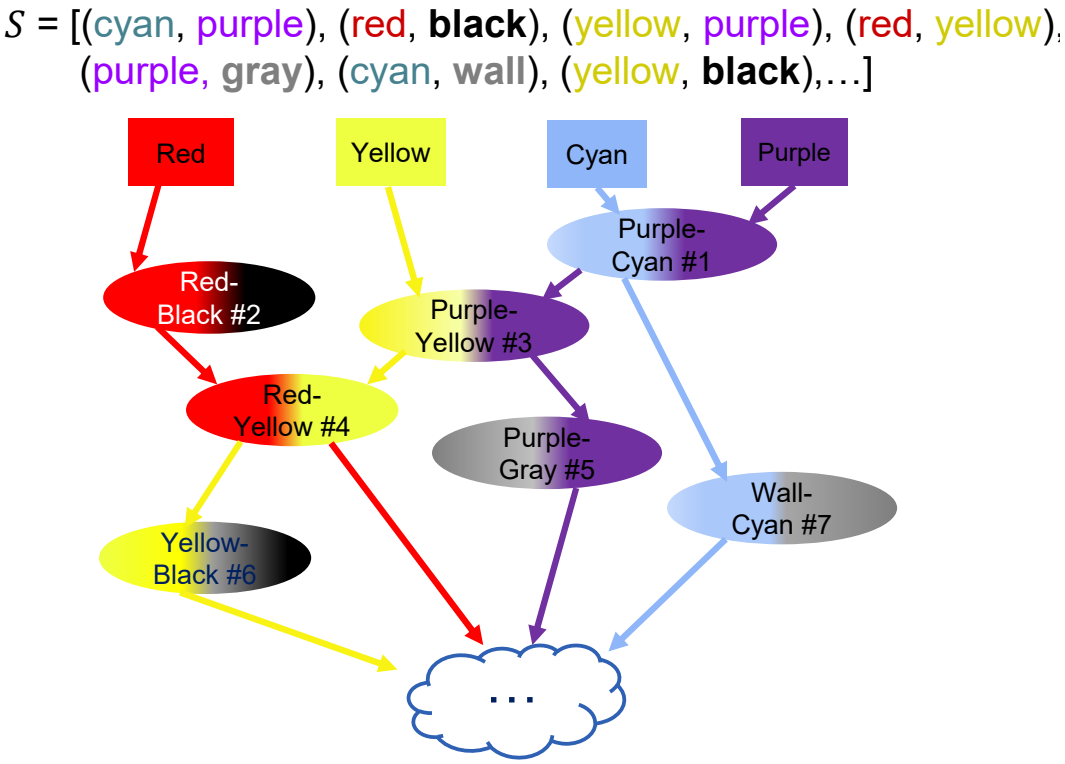

Figure A.3: Illustrates transforming a sequence of events (top) to a DAG (bottom). It corresponds to the video in Figure 1 bottom.

Using the main dataset demonstrate a similar trend (See appendix K). We discuss the baselines' in Appendix A.1, and we provide qualitative examples in Appendix B.

We report the "count" and "bottleneck" ablations by zeroing their respective features in the instruction and using the same model weights that were used to report the performance of the ROSETTE model. We did not retrain the model for these cases because the ROSETTE model was trained to handle these cases, as is evident by the "Unconstained" metric.

For ablating the "full" instruction, we retrained the model, while completely zeroing the representation vector of the input instruction.

E Implementation details of the model of the score function

A model for the score function. The model takes as inputs the instruction g and sequence of events S_u , and predicts a scalar score $v(u)$. A naive approach is to represent S_u as a sequence. However, such representation may not convey well the relations describing the cascade of events. For illustration, in the following sequence of collision events *[(A, B), (C, D), (A, E)]*, the collision (A,E) is driven by (A,B), because A is common for both, while (C,D) is less relevant for describing the events that lead to (A,E). Instead, we transform each sequence to a Directed Acyclic Graph (DAG) that captures relations in the cascade of events (Figure A.3).

We use a Graph Neural Network (GNN) to parameterize our score function. We represent the graph as a tuple (A, X, E, z) where $A \in \{0,1\}^{n\times n}$ is the graph adjacency matrix, $Y \in \mathbb{R}^{n\times d}$ is a node feature matrix, $E \in \mathbb{R}^{m\times d'}$ is an edge feature matrix, and $z \in \mathbb{R}^{d''}$ is a global graph feature. we chose to use a popular message passing GNN model (Battaglia et al., 2018) that maintains learnable node, edge and global graph representations.

Architecture The model is composed of several message passing layers, $L^k \circ \cdots \circ L^1$ where each L^i updates all representations, i.e.:

$$X^{i+1}, E^{i+1}, z^{i+1} = L^i(A, X^i, E^i, z^i; \theta^i),$$

Each layer L_i updates the features sequentially: the node and edge features are updated by aggregating local information, while the global feature is updated by aggregating over the whole graph. We denote the parameters of the MLPs that are used in a layer L_i as θ_i, and note that these are the only learnable parameters in the model. At the last layer $i = k$ we use a single dimension for the global feature, i.e., $d' = 1$, which is then used as the score of the event node.

Feature representation We describe next the feature representation of the inputs to the node feature matrix Y, the edge feature matrix E, and the global graph feature z.

We start by describing a feature representation of any of the dynamic and static objects in the scene: An object o feature representation, noted by $obj\_feat(o)$, is a concatenation of the following fields

$$\begin{aligned} obj\_feat(o) = [&one\_hot(o), is\_stationary, is\_active, \\ &instruct\_inner\_prod, bottleneck\_ind, count, count\_ind], \end{aligned} \tag{1}$$

where $one\_hot(o)$ is a one-hot vector $\in \mathbb{R}^{12}$, as represented by the instruction; $is\_stationary$ indicates whether the object is stationary; is_active means that in the context of a current collision, the object dynamics were coming from a collision chain that included the pivot; $instruct\_inner\_prod$ is the results of an inner product of $one\_hot(o)$ with each of the 5 object representations at the instruction embedding (Section H.3). Finally, $bottleneck\_ind, count, count\_ind$ are copied from the instruction embedding.

The graph node and edge features are derived from the DAG representation (Figure A.3). Each row of the node feature matrix Y concatenates the two objects that participate at a collision $[obj\_feat(obj_a), obj\_feat(obj_b)]$. Each row at the edge feature matrix E represents $obj\_feat(o)$ of the object on that edge.

Last, the global feature z is a copy of the instruction embedding Eq. (4).

Training data For calculating the training labels of the score function, we traverse the semantic tree along the ground-truth sequence of the solution cascade and collect the *positive* labels using Eq. (**??**). If the event tree cannot reproduce the solution sequence of a sample (due to errors accumulated by the event-driven forward model), then Eq. (**??**) cannot be calculated, and we drop that sample from the training set. We collect *negative* examples (with $V = 0$) by (1) taking the child nodes that diverge from the path to the ground-truth solution. (2) Traverse a random path along the tree with the same length as the ground truth sequence, and set the score of all the nodes along that path to 0. Note that setting the scores of every node along these paths to $V = 0$ is a heuristic and may introduce some label noise with respect to negative examples. Additional research may be required to analyze the label-noise consequences and address it.

F COUNTERFACTUAL UPDATE FOR THE SCORE FUNCTION

In this section, we derive the expression of the score function update according to the observed cascade (Eq. (**??**)). We start the derivation by repeating the preliminary derivation steps introduced in the main text in more detail.

During inference, we observe a cascade that does not satisfy the instruction, and are asked to retrospectively suggest a better solution. How can the information can be used to find a better solution? The probabilistic score function allows us to formalize this problem in a Bayesian setting. We treat the model predictions as a *prior* for the true score, and the information about the observed cascade as *evidence*. We then ask how to update the score function given the observed evidence. Formally, we condition Eq. (**??**) by the evidence, $V(u|S_{u^{obs}}$ doesn't satisfy $g)$.

We denote the set of interventions that satisfy the instruction g as $\mathcal{G}_g \subset \mathcal{Y}$, and the evidence by E. Note that an equivalent definition for the *unconditioned* score function $V(\cdot)$ is

$$\begin{aligned} V(u) &= \Pr\left(Q(y) \text{ satisfies } g | y \in Y_u, g\right) \\ &= \Pr\left(y \in \mathcal{G}_g | y \sim U\left(Y_u\right)\right) \end{aligned}$$

Our evidence is that for a particular $\tilde{y} \in Y_{obs}$, we have $\tilde{y} \notin \mathcal{G}_g$. Now, by definition, every $y, y' \in Y_{obs}$ share the same observed cascade $S_{u^{obs}}$. Therefore, the evidence E can be equally formulated as $y' \notin \mathcal{G}_g$ for any y' sampled uniformly from $Y_{u^{obs}}$, $y' \sim U(Y_{u^{obs}})$. For brevity, we set $Y_{obs} = Y_{u^{obs}}$.

The *conditioned* score function is then,

$$\Pr\left(y \in \mathcal{G}_g | y \sim U\left(Y_u\right), E\right)$$

We use the law of total probability and write,

$$\begin{aligned}
&\Pr\left(y \in \mathcal{G}_g | y \sim U\left(Y_u\right), E\right) \\
=&\Pr\left(y \in \mathcal{G}_g y \sim U\left(Y_u\right), E, y \in Y_{obs}\right) \Pr\left(y \in Y_{obs} | y \sim U\left(Y_u\right), E\right) \\
+&\Pr\left(y \in \mathcal{G}_g | y \sim U\left(Y_u\right), E, y \in Y_{obs}^c\right) \Pr\left(y \in Y_{obs}^c | y \sim U\left(Y_u\right), E\right) \\
=&\Pr\left(y \in \mathcal{G}_g | y \sim U\left(Y_u \cap Y_{obs}\right), E\right) \Pr\left(y \in Y_{obs} | y \sim U\left(Y_u\right), E\right) \\
+&\Pr\left(y \in \mathcal{G}_g | y \sim U\left(Y_u \cap Y_{obs}^c\right), E\right) \Pr\left(y \in Y_{obs}^c | y \sim U\left(Y_u\right), E\right)
\end{aligned}$$

Furthermore,

$$\begin{aligned}
\Pr\left(y \in Y_{obs} | y \sim U\left(Y_u\right), E\right) &= \Pr\left(y \in Y_{obs} | y \sim U\left(Y_u\right)\right) \\
\Pr\left(y \in Y_{obs}^c | y \sim U\left(Y_u\right), E\right) &= \Pr\left(y \in Y_{obs}^c | y \sim U\left(Y_u\right)\right)
\end{aligned}$$

As the conditioned event $y \in Y_{obs}$ is independent of E.

The relations between node U^{obs} and u can be one of the three: a) the observed node is a descendant of u (and therefore $Y_u \cap Y_{obs} = Y_u$) b) u and the observed node belong to different branches, and therefore $Y_u \cap Y_{obs} = \emptyset$, or c) u is a descendant of the observed node (and therefore $Y_u \cap Y_{obs} = Y_{obs}$). However, u^{obs} represents a complete cascade rather than a partial sequence, and therefore the observed node does have any children, and we can ignore c).

Let us consider each case separately.

u **and the observed node are along different paths**. In this case,

$$\begin{aligned}
Y_u \cap Y_{obs} &= \emptyset \\
Y_u \cap Y_{obs}^c &= Y_u \\
\Pr\left(y \in Y_{obs}^c | y \sim U\left(Y_u\right)\right) &= 1 \\
\Pr\left(y \in Y_{obs} | y \sim U\left(Y_u\right)\right) &= 0,
\end{aligned}$$

and we're left to evaluate $Pr\left(y \in \mathcal{G}_g | y \sim U\left(Y_u\right), E\right)$. Since the evidence in this case provides information about a set that y is not conditioned on, it is independent of y, and therefore we conclude with,

$$\Pr\left(y \in \mathcal{G}_g | y \sim U\left(Y_u\right), E\right) = \Pr\left(y \in \mathcal{G}_g | y \sim U\left(Y_u\right)\right) = V(u)$$

u **is a descendant of the observed node.** Here,

$$\begin{aligned}
Y_u \cap Y_{obs} &= Y_{obs} \\
\Pr\left(y \in Y_{obs} | y \sim U\left(Y_u\right)\right) &= fr(y_{obs}, y_u)
\end{aligned}$$

In this case,

$$\begin{aligned}
&\Pr\left(y \in \mathcal{G}_g | y \sim U\left(Y_u\right), E\right) \\
=&\Pr\left(y \in \mathcal{G}_g | y \sim U\left(Y_u \cap Y_{obs}\right), E\right) fr(y_{obs}, y_u) \\
+&\Pr\left(y \in \mathcal{G}_g | y \sim U\left(Y_u \cap Y_{obs}^c\right), E\right) \left(1 - fr(y_{obs}, y_u)\right) \\
=&\Pr\left(y \in \mathcal{G}_g | y \sim U\left(Y_{obs}\right), E\right) fr(y_{obs}, y_u) \\
+&\Pr\left(y \in \mathcal{G}_g | y \sim U\left(Y_u \cap Y_{obs}^c\right), E\right) \left(1 - fr(y_{obs}, y_u)\right) \qquad (2)
\end{aligned}$$

Now,

$$\begin{aligned}&\Pr\left(y \in \mathcal{G}_g | y \sim U\left(Y_{obs}\right), E\right)\\ =&\Pr\left(y \in \mathcal{G}_g | y \sim U\left(Y_{obs}\right), \{\forall y' \in Y_{obs}, y' \notin \mathcal{G}_g\}\right)\\ =&0\end{aligned}$$

Since the evidence indicates that for every $y' \in Y_{obs}$ the resulting sequence $S_{u^{obs}}$ does not satisfy the goal. Furthermore,

$$\Pr\left(y \in \mathcal{G}_g | y \sim U\left(Y_u \cap Y_{obs}^c\right), E\right) = \Pr\left(y \in \mathcal{G}_g | y \sim U\left(Y_u \cap Y_{obs}^c\right)\right) \tag{3}$$

As E does not add information when we sample from $(Y_u \cap Y_{obs}^c)$.

Therefore,

$$\Pr\left(y \in \mathcal{G}_g | y \sim U\left(Y_u\right), E\right) = \Pr\left(y \in \mathcal{G}_g | y \sim U\left(Y_u \cap Y_{obs}^c\right)\right)\left(1 - fr(y_{obs}, y_u)\right)$$

Now

$$\begin{aligned}\Pr\left(y \in \mathcal{G}_g | y \sim U\left(Y_u\right)\right) = &\Pr\left(y \in \mathcal{G}_g | y \sim U\left(Y_u \cap Y_{obs}\right)\right) fr(y_{obs}, y_u)\\ &+ \Pr\left(y \in \mathcal{G}_g | y \sim U\left(Y_u \cap Y_{obs}^c\right)\right)\left(1 - fr(y_{obs}, y_u)\right)\end{aligned}$$

Namely,

$$V(u) = V(u_{obs}) \cdot fr(y_{obs}, y_u) + \Pr\left(y \in \mathcal{G}_g | y \sim U\left(Y_u \cap Y_{obs}^c\right)\right)\left(1 - fr(y_{obs}, y_u)\right)$$

or

$$\Pr\left(y \in \mathcal{G}_g | y \sim U\left(Y_u \cap Y_{obs}^c\right)\right) = \frac{V(u) - V(u_{obs}) \cdot fr(y_{obs}, y_u)}{1 - fr(y_{obs}, y_u)}.$$

Plugging this back to Eq. 3 we obtain:

$$\Pr\left(y \in \mathcal{G}_g | y \sim U\left(Y_{obs}\right), E\right) = V(u) - V(u_{obs}) \cdot fr(y_{obs}, y_u)$$

which is our final result.

G Relation to Causal-Inference

The DAG representation (Section 3) is useful for graphically representing one instance of a cascade, but we intentionally avoid naming it a *Causal* DAG, because it can't represent dependencies between events that are not explicitly observed in the video. E.g., in the example *[(A, B), (C, D), (A, E)]* in Section 3, it may be that (A,E) depends on (C,D) because C blocks D from reaching to E before A do. The event tree can simulate this behaviour, while the DAG (C,D) ; (A,B)-¿(A,E) is unaware of it. From a formal causal inference perspective (Pearl, 2000), our event tree is the part of our approach that can be related to the formal "Structured" Causal Model (SCM). As it is a generative model that reflects the data generation process; it can account for complex dependencies between events; and every edge corresponds to a function, namely, the event-driven forward model.

H Data generation details

H.1 Video generation details

In this section, we describe the generation process of the dynamical scene. We first create an "unperturbed" video. Then, we perturb the video by modifying the velocity of a specific element, which will be later designated as the pivot. We let the perturbed video roll out, validate that it

is indeed semantically different than the unperturbed video, and label it as the "observed" video. The unperturbed video can now be used as reference for our instruction generation process. It is a realization of a specific, complex, semantic chain of events that is both semantically different than the perturbed ("observed") video and is also feasible, e.g, by setting the intervention value as to revert the perturbation. This flow guarantees that we can ask meaningful instructions on the "observed" that are guaranteed to be realizable.

The unperturbed video. We construct the unperturbed video by iteratively adding spheres and collisions in a physical simulator (IsaacGym (Makoviychuk et al., 2021)) increasing the video complexity. We start by placing a sphere in the confined four-walled space and assign it a random velocity.

The dynamics of a sphere moving freely in a confined square area can be expressed analytically. We pick a random time t_1, hitting velocity, and hitting angle for the first collision. We analytically solve for the initial position and velocity at $t_0 = 0$ that will result in the a collision at t_1 with the specific hitting velocity and angle. We assign these value to a randomly colored sphere.

Due to discrepancies between the simulator dynamics and the kinematic analytic model, we roll out the dynamical system in the simulator, and record the system state immediately after a collision.

We continue adding spheres iteratively. Given a state at t_i, we randomly select a sphere O_i from the existing spheres, collision time t_{i+1}, hitting angle and velocity. We solve analytically and find the initial position and velocity at $t_0 = 0$ that will result in a collision with O_i corresponding parameters. We roll out the dynamical system, and update the velocities and positions records after each collision with the empirical values from the simulator.

Our simple kinematic model assumes the target sphere and the newly added move freely. However, other spheres may cross their trajectories, resulting in an a collision that will distract the spheres from their designated path. However, this simply means that the planned random collision was replaced by a different collision. Since we update our records of the resulting collisions and corresponding output velocities and positions using the simulator, this does not pose any serious limitations.

The observed video. We pick a random sphere from the set of spheres and assign it a different velocity at $t = 0$. We roll out the system in the simulator and log all resulting collisions. We validate that the resulting collision sequence is different than the unperturbed video collision sequence. We now have two videos that differ only in the initial velocity of a specific sphere, but result in a substantially different semantic chain of events.

H.2 Instruction generation details

We describe the instruction generation process when given an "observed" video, and a "counterfactual" video that displays an alternative cascade of events.

Given a ground-truth video, its sequence of collisions, and a pivot, we randomly sample an instruction: Starting by randomly sampling a target collision from the sequence. And then, we randomly sample up to two constraints that accompany the goal. For constructing the constraints, we first represent the sequence of collisions using a DAG, in a similar fashion as described in Figure A.3, then we use standard NetworkX functionality (Hagberg et al., 2008) for graph traversal: (1) We use "dag.ancestors()" to get a list of nodes for the "bottleneck" constraint. (2) We use "all_simple_paths()" to count the nodes in a chain reaction between the pivot and the target collision.

To avoid trivial goals, we drop an instruction if it is fulfilled by the observed video (rather than the "counterfactual" video). We sample up to 5 unique instructions for each scene ($\sim$4 on average).

H.3 Instruction feature representation

We assume perfect lexical perception, and provide the agent with the a structured vector representation of each instruction, by concatenating the following fields:

$$instruction\_emb = [target\_obj\_a, target\_obj\_b, pivot\_obj, bottleneck\_obj\_a, \\ bottleneck\_obj\_b, bottleneck\_ind, count, count\_ind], \quad (4)$$

where $target\_obj\_a, target\_obj\_b$ are the object representations of the target collision. $pivot\_obj$ represents the pivot. $bottleneck\_obj\_a, bottleneck\_obj\_b, bottleneck\_ind$ represent the two "bottle-

neck" objects and a binary indicator scalar. If an "bottleneck" constraint is not applicable for an instruction, we them all to 0. $count, count\_ind$ are 2 scalar values: One for the number of collisions of the chain "count" constraint, and another used as a binary indicator for the "count" constraint. Similarly if a "count" constraint is not applicable for an instruction, we set both $count$ and $count\_ind$ to 0.

Finally, note that each object is represented by a one-hot vector $\in \mathbb{R}^{12}$, because the environment has 12 types of unique objects: 6 colored balls, 2 static pins, and 4 walls.

H.4 Complex instructions dataset

For the complex instructions dataset, we add a third object centric constraint that counts the number of interactions a specific object makes on the paths from the pivot to the target collision. It resembles constraining the amount of resources available per instance on a logistic chain. With an additional constraint we can test our approach on a more challenging task that has a large variety of instructions that have 2 or more constraints. We split the evaluation set to "Hard" instructions that have 2 or more constraints, and "Easy" instruction with 0-1 constraints. We generated instructions for the same scenes as in the main dataset, which yields $\sim$4.5 instructions per scene. The test set consists of 2190 episodes, where 54% are "Hard" instructions.

I The forward model

In our physical setup, the dynamics are prescribed by the position and velocity $c_i^j = (pos_i^j, vel_i^j), j = 1 \dots n$ of each of n objects in the environment. The world state w_i^u of a node u is then a tuple

$$w_i^u = (c_i^1, c_i^2, ...c_i^n, t_i), \tag{5}$$

where for the root node $t_i = 0$ for all x_i.

The forward module takes as input a world state w_i it outputs the next semantic event (s'), and a state $f(w_i) = w_i' = ({c'}_i^1, {c'}_i^2, ...{c'}_i^n, t_i')$ immediately after the predicted semantic event at t_i'. The section is divided into three parts. First, we describe the analytical equations that control if two objects will collide. Then we show how can leverage the analytic model to efficiently branch out from a node in the event tree. Finally, we fill in the missing details and present the full forward model.

The collision detector. Assume two spheres $i = \alpha, \beta$ moving freely on a plane with an initial velocity of $\mathbf{v_i}$ and position $\mathbf{r_i}$ at $t = 0$. Each sphere has a radius of l_i. If the two sphere collide, then, at the moment of collision, the spheres intersect at a single point. We can use a simple geometric calculation to find their *planar* distance. The distance between the center of spheres is $l_\alpha + l_\beta$, while the vertical distance between the two centers is $|l_\alpha - l_\beta|$. The resulting planar distance is then:

$$d = \sqrt{(l_\alpha + l_\beta)^2 - (l_\alpha - l_\beta)^2} = 2\sqrt{l_\alpha l_\beta}. \tag{6}$$

Therefore, in order to check if the spheres collide, we can check if the planar distance between the two spheres is ever equal to d,

$$\|\mathbf{r}(t)\|^2 = \|\mathbf{r}_\alpha + \mathbf{v}_\alpha \cdot t - \mathbf{r}_\beta - \mathbf{v}_\beta \cdot t\|^2 = d^2 \tag{7}$$

This is a quadratic equation in t, which we can solve for analytically. If the discriminant is non-negative, the collision time corresponds to the smaller root. The spheres' velocities immediately after the collision are given by:

$$\mathbf{v_1'} = \mathbf{v_1} - \frac{2m_2}{m_1 + m_2} \frac{\langle \mathbf{v_1} - \mathbf{v_2}, \mathbf{y_1} - \mathbf{y_2} \rangle}{\|\mathbf{y_1} - \mathbf{y_2}\|^2} \cdot (\mathbf{y_1} - \mathbf{y_2}) \tag{8}$$

$$\mathbf{v_2'} = \mathbf{v_2} - \frac{2m_2}{m_1 + m_2} \frac{\langle \mathbf{v_1} - \mathbf{v_2}, \mathbf{y_1} - \mathbf{y_2} \rangle}{\|\mathbf{y_1} - \mathbf{y_2}\|^2} \cdot (\mathbf{y_2} - \mathbf{y_1}) \tag{9}$$

Likewise, it is trivial to obtain an analytical expression for the collision time and output velocity of a collision between a freely moving sphere and each of the static walls bounding the spheres (should

the collision occur). The sphere's velocity in the direction orthogonal to the walls flips, while the parallel velocity remains the same.

Parallelizing collision detection. The collision detector provides an analytic condition that validates whether a specific collision occurs.

$$(\Delta\mathbf{r}\cdot\Delta\mathbf{v})^2 - 4(\|\Delta\mathbf{r}\|^2 - d^2)\|\Delta\mathbf{v}\|^2 > 0 \tag{10}$$

Eqs. 6-10 can be solved in parallel for multiple tuples of $(\mathbf{r_1}, \mathbf{v_1}, \mathbf{r_2}, \mathbf{v_2})$ on a GPU using packages such as PyTorch. Given an intervention set of Y_u, and a corresponding world-state set W_u, we iterate over all possible collisions $S_{ij} = (O_i, O_j)$. For each collision between object i and j we can apply our collision detector by extracting the corresponding coordinates c_w^i, c_w^j, t_w from $w \in W_u$ (Eq 5). We can do in parallel for all world states $w \in W_u$. If a collision is predicted, we construct a new node child u' of u. We associate with it the interventions for which the collision detector returned a non-null time for the collision, Y'_u, the corresponding set of post-collision world state W'_u, and the event sequence $S'_u = concat(S_u, (O_i, O_j))$

The complexity is quadratic in the number of object rather than linear in the number of interventions. This allows us to apply our algorithm with a high number of interventions, and therefore enable us to consider delicate sequences of collision that would require refined "trick shots".

This approach considers every two objects O_i, O_j as moving freely. However, another object in the environment, e.g, O_k, may interact with O_i (without loss of generality) before the collision. This necessarily means that the collision time t_{ik} precedes t_{ij}. In order to account for this, we hold an additional structure that maintains the minimal collision time for every $w \in W_u$. We update it as we iterate over all possible collisions. Then, we associate each $w \in W_u$ and its corresponding $y \in Y_u$ to the event node corresponding to the collision with the earliest collision time.

J Additional setups

Here, we present examples for additional setups for which our formalism can be applied.

J.1 Logisitics

While logistics is a complex field, we describe a simple model that captures the essential components of a logistics problem.

Consider a large logistics enterprise that needs to coordinate shipping from multiple locations. The enterprise has multiple carriers (e.g, trucks or airplanes) $v_i, i = 1..m$ and routes them between logistic centers at $r_j, j = 1..n$.

A plan is a schedule for each carrier τ_j, where a schedule τ_j is a sequence of arrivals and departures between various logistic centers,

$$\tau_j = \{(r_j^0, t_{in}^0, t_{out}^0), (r_j^1, t_{in}^1, t_{out}^1), ...\}$$

Not all plans are *feasible*. Each carrier can travel at a range of velocities, resulting in a range of arrival times to the possible destinations. Carriers can exchange cargo is they are present at the same logistic center.

Now, assume a logistic center is suddenly shut down. Rescheduling all carriers is unfeasible, as some may be already committed to a route, or may not be easily diverted (e.g., are airborne). Furthermore, recomputing a new plan for the complete enterprise might be computationally heavy. Finally, it seems reasonable that re-planning of only the routes of carriers that were suppose to arrive to the closed logistic center may be enough. We denote those k carriers as the *rescheduled carriers*. Note that while only some of routes may be re-planned, other carriers might be affected as well due to a cascade of delays or even cargo exchange cancellations.

Such re-planning may be constrained by semantic instruction. For example: "Carrier X should only make two deliveries", "Carrier Y should meet carrier Z before meeting Carrier W", etc. .

We now cast this problem into our general framework, described in Section 3. An event is the arrival or departure of a carrier to a logistic center. Each intervention $y \in \mathcal{Y}$ is a set of plans the rescheduled carriers,

$$y = (\tau_0, \tau_1, ..., \tau_k).$$

A world state w_j is the position of the k carriers at different time $((p_j^0, t_j^0), ..., (p_j^k, t_j^k))$ The forward model takes as input a world state and outputs all world state that obey the following two rules: 1) At least one carrier moved to a different logistic center. 2) The transition of carriers follow physical constraints. If carrier i can move at velocity range $[v_{min}^i, v_{max}^i]$ and it moves between two logistics centers r_a and r_b, then the transition time must be in

$$\left[\frac{\|r_a - r_b\|}{v_{max}^i}, \frac{\|r_a - r_b\|}{v_{min}^i} \right]. \tag{11}$$

For simplicity, we assume that there is no cargo limit.

The expressions for the induced probability, Eqs. **??** -**??**, remains the same.

J.2 Failure cascades in power grids

Cascading failures in power grid may cause large blackout with substantial economical damage Schäfer et al. (2018). Cascading Power failures may be induced due to random fluctuations and can develop on orders of seconds. Human operators or complex control mechanism may not be able react in time. The transmission system operator may use an event-driven forward model to find fast automated reactions for unseen dynamical configurations to avoid cascading failures.

Here, semantic events are failures of nodes (nodes; e.g., transformers, power generators, etc.) or power lines (edges). Power flow follows a known set of ODE for a given grid (eqs 14-15 in Schäfer et al. (2018)):

$$\frac{\mathrm{d}}{\mathrm{d}t}\theta_i = \omega_i, \tag{12}$$

$$I_i \frac{\mathrm{d}}{\mathrm{d}t}\omega_i = P_i - \gamma_i \omega_i + \sum_{j=1}^{N} K_{ij} \sin\left(\theta_j - \theta_i\right), \tag{13}$$

where, θ_i, ω_i are the dynamical variable at node i, P_i is the power input (or output) at node i, and K_{ij} is a weighted adjacency matrix representing the grid connectivity. If at some point in time the flow $F_i j$ exceeds the powerline capacity $\alpha k_{ij}, \alpha \in [0, 1]$ (eqs 1-2), the line fails. This condition can be formally written as

$$F_{ij}\left(t\right) = K_{ij} \sin\left(\theta_j\left(t\right) - \theta_i\left(t\right)\right) > \alpha K_{ij}.$$

If the line fails, the dynamics are governed by a new effective coupling matrix $K_i j$, and the dynamics in Eqs. 12-13 changes accordingly.

A failure of a node may induce outage to some region. The transmission system operator (TSO) might define goals such as "no more than three failures", "the maximal number of affected people should be less than n", "these highly important nodes should not fail" etc.

J.3 Evolution of natural disasters

Finally, another use case is the evolution of natural disasters. Zuccaro et al. (2018) provides a full description of an event tree. It models transitions between events like a "seismic shock" which can lead to "landslide" and result with "traffic accident", and how taking preventive measures like "evacuate population" can influence the total damage caused by the crisis.

K Complex scenario conditioning for the main dataset

In Figure A.4 we provide the results for complex scenario conditioning for the main dataset (with two type of constraints). The results demonstrate a similar trend as in the complex instruction dataset in Figure **??**.

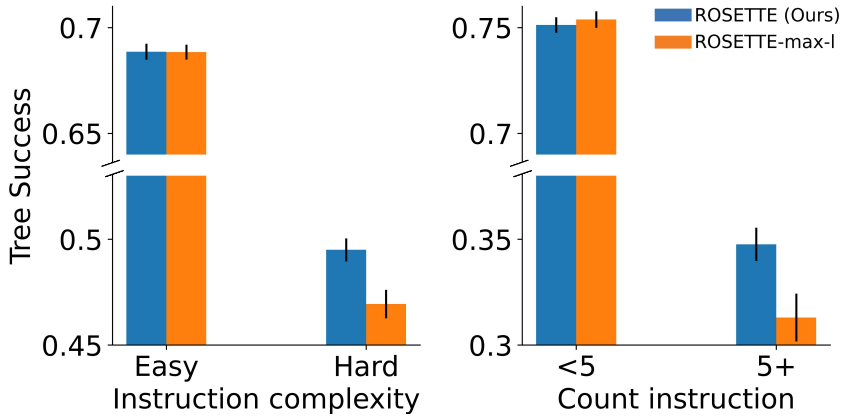

Figure A.4: Comparing "Counterfactual" search (ROSETTE) with "Maximum likelihood" search (ROSETTE-max-l) for 2 levels of instruction complexity ("Hard": 2 or more constraints) and for two levels of "count" instructions ("5+": 5 or more). **Here we use the main dataset.** Using the observed cascade, ROSETTE performs better in complex scenarios.